ACS Catalysis

Research Article

pubs.acs.org/acscatalysis

Catalysis and In Situ Studies of Rh_1/Co_3O_4 Nanorods in Reduction of NO with H_2

Lei Wang,[∥,†,⊥] Shiran Zhang,[∥,†] Yuan Zhu,[†] Anitha Patlolla,[‡] Junjun Shan,[†] Hideto Yoshida,[§] Seiji Takeda,[§] Anatoly I. Frenkel,[‡] and Franklin (Feng) Tao*[,†]

[†]Department of Chemistry and Biochemistry, University of Notre Dame, Notre Dame, Indiana 46556, United States

[‡]Department of Physics, Yeshiva University, New York, New York 10016, United States

[§]Institute of Scientific and Industrial Research, Osaka University, Osaka 567-0047, Japan

Supporting Information

ABSTRACT: Efficient use of precious metal atoms in heterogeneous catalysis is important in chemical transformation and environmental remediation. Co_3O_4 with singly dispersed Rh atoms, Rh_1/Co_3O_4, was synthesized for reduction of nitric oxide with hydrogen. Studies using extended X-ray absorption fine structure (EXAFS) showed that the singly dispersed Rh atoms are bonded to surface oxygen atoms before catalysis. In situ studies using ambient pressure X-ray photoelectron spectroscopy (AP-XPS), EXAFS, and X-ray Absorption Near Edge Structure (XANES) suggested that the surface of Rh_1/Co_3O_4 with singly dispersed Rh atoms is restructured into a new geometry at 220 °C in the mixture of reactant gases (NO and H_2). It forms $RhCo_n$ nanoclusters singly dispersed in the surface layer of Co_3O_4. The restructured catalyst, $RhCo_n/Co_3O_4$ exhibits a much better catalytic performance in contrast to Rh_1/Co_3O_4 without a restructuring. $RhCo_n/Co_3O_4$ is highly active for reduction of nitric oxide with hydrogen. Selectivity to the production of N_2 at 220 °C is 87% and reaches 97% at 300 °C. In situ studies showed this catalyst maintains its single dispersion of Rh atoms up to 300 °C during catalysis.

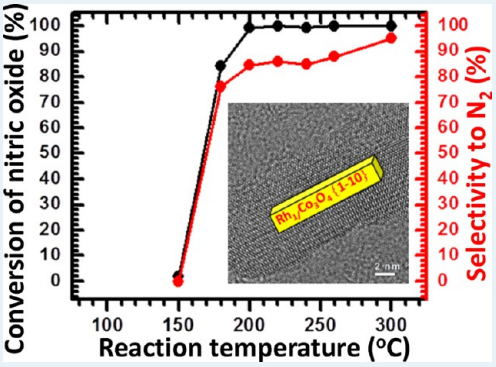

KEYWORDS: *nanocatalysis, in situ study, Co_3O_4, ambient pressure XPS, nitric oxide*

1. INTRODUCTION

Noble metal nanoparticles supported on oxides are important catalysts for chemical transformation, energy conversion, and environmental remediation.[1−17] For example, Rh and Pt are key components of commercial catalysts in the reduction of nitric oxide.[18−24] From the point of view of practical applications at the industrial scale, these catalysts are prohibitively expensive. With colloidal synthesis, the size of precious metal particles can be decreased to a few nanometers or even one nanometer, which significantly increases the surface to volume ratio.[25−39] To fully use the precious metal catalysts, another solution is the use of catalysts with a single dispersion of precious metal atoms under the assumption that the single dispersion of precious metal atoms does not significantly degrade its catalytic activity and selectivity. Thus, design of a catalyst with a single dispersion of a precious metal which is highly selective in the production of ideal product(s) without loss of catalytic activity is an ideal solution but remains very challenging for many catalytic reactions. Driven by this motivation, we have here prepared Co_3O_4 with singly dispersed Rh atoms and performed in situ studies of their surface chemistry and structure during catalysis toward a demonstration of the development of singly dispersed catalysts with enhanced catalytic performance through incorporation of in situ studies into the process.

A catalyst with singly dispersed Rh atoms on the surface of Co_3O_4, Rh_1/Co_3O_4, was prepared by impregnation. The atomic ratio of Rh to Co in precursors of the synthesis is 0.1%. Rh ions are dispersed on Co_3O_4 nanorods followed with a reduction. The single dispersion of Rh atoms on Co_3O_4 was confirmed with EXAFS. This catalyst exhibits higher selectivity to production of N_2 in reduction of nitric oxide with hydrogen in the temperature regime of 180 to 300 °C. In situ studies using AP-XPS and EXAFS revealed the formation of new active $RhCo_n$ nanoclusters integrated in the Co_3O_4 surface. This new active phase is thermodynamically stable up to 300 °C.

2. EXPERIMENTAL SECTION

Catalyst Synthesis. Synthesis of Co_3O_4 nanorods with singly dispersed Rh atoms includes three steps: synthesis of Co_3O_4 nanorods, impregnation of Rh^{3+} on the surface of Co_3O_4 nanorods, and on-site reduction of Rh^{3+} followed with a surface binding to oxygen atoms. Co_3O_4 nanorods were prepared by the calcination of a cobalt hydroxide carbonate precursor obtained by the precipitation of 2.49 g of cobalt(II)

Received: December 15, 2012
Revised: March 19, 2013
Published: March 26, 2013

 © 2013 American Chemical Society

acetate tetrahydrate (≥99.0%, Aldrich) with sodium carbonate (>99.95%, Aldrich) in 30 mL of ethylene glycol (99.8%, Aldrich). The preparation of pure Co_3O_4 nanorods is a modification of one developed in the literature.[40] When cobalt acetate was mixed with ethylene glycol at 160 °C, the $-OCH_2-CH_2O-$ chain was tightly bound with the cobalt cations. The addition of aqueous sodium carbonate solution (0.2 M) resulted in the formation of a solid cobalt hydroxide carbonate incorporating ethylene glycol, having the shape of a nanorod. A following calcination of the precursor at 350 °C in air for 3 h with a ramping rate of 2 °C/min forms well crystallized Co_3O_4 nanorods.

A 0.71 g portion of $Rh(NO_3)_3$ (~36% Rh basis, Aldrich) was dissolved in 150 mL of deionized water. The concentration of Rh^{3+} is 0.51 wt %. A 0.70 g portion of Co_3O_4 nanorods was dispersed in 15.0 g of water. $Rh(NO_3)_3$ aqueous solution was added to a methanol solution of dispersed Co_3O_4 nanorods. The atomic ratio of Rh to Co is 0.1%. Vigorous stirring is necessary to ensure a homogeneous impregnation of Rh^{3+} on the surface of Co_3O_4 nanorods. Then, 0.016 g of $NaBH_4$ (99%, Aldrich) dissolved in water was dropwise added to the solution of Co_3O_4 nanorods with Rh^{3+} for a reduction of Rh^{3+}. Upon reduction, a Rh atom immediately bonds to the surface of Co_3O_4 nanorods, avoiding aggregation. The solution of Co_3O_4 nanorods loaded with Rh atoms was filtered. The precipitate was washed thoroughly with deionized water and ethanol (99.5%, Aldrich) to remove the soluble ions, was dried, and kept for applications.

Characterization of Catalysts Ex Situ. The amount of Rh_1/Co_3O_4 nanorods was measured with inductively coupled plasma (ICP) analysis. Size, shape, and lattice fringes of pure Co_3O_4 and Rh_1/Co_3O_4 catalysts synthesized were identified with Titan TEM (FEI Titan 80−300, 300 kV FEG TEM with point resolution 0.2 Å). HAADF-STEM images were collected on JEOL JEM-ARM 200F with a CEOS probe corrector by the Takeda group at Osaka University in Japan. The used accelerating voltage is 200 kV. The HAADF-STEM resolution is 0.1 nm. X-ray diffraction (XRD) of Co_3O_4 nanorods was performed with synchrotron radiation with a beam wavelength of 0.3196 Å at the National Synchrotron Light Source, Brookhaven National Laboratory. Ex-situ XPS studies of Co_3O_4 and Rh_1/Co_3O_4 catalysts were performed on the ambient pressure X-ray photoelectron spectroscopy system in the Tao group.

Characterization Using in Situ Techniques. Ambient pressure XPS (AP-XPS) studies were performed on the in-house AP-XPS system in the Tao group.[41−44] Catalyst samples are transferred into a reaction cell which has a gas inlet and outlet for in situ studies with a flowing mode. The reactant environment of the in situ studies of Rh_1/Co_3O_4 catalyst is a mixture of 1 Torr NO (99.99% NO, Praxair) and 1 Torr of H_2 (99.99%, Praxair). Rh 3d, Co 2p, O 1s, and Au 4f were collected in the reaction environment at different temperatures. Au 4f of the substrate of gold foil was always taken as a reference after data acquisition at each reaction condition. Gas composition during catalysis in the reaction cell is monitored and analyzed online by using the mass spectrometer installed at lens 1 of the differential pumping stages of the AP-XPS system.

In situ X-ray absorption spectroscopy measurements were performed at the beamline X-18B at the National Synchrotron Light Source, Brookhaven National Laboratory. The storage ring energy was 2.5 GeV, and the ring current was in the range of 110−300 mA. A double-crystal Si (111) monochromator was used to scan X-ray energy between 150 eV below and 970 eV above the Rh K edge energy (23220 eV). The samples were made by pressing the powders into circular pellets using a hydraulic press and transferred onto a sample holder of a Nashner−Adler in situ cell.[45] The cell is capable of heating the sample under a controlled atmosphere up to 600 °C. The X-ray absorption coefficient in metallic Rh foil was measured in reference mode for X-ray energy calibration and data alignment. Up to five consecutive scans were collected at each stage of the reaction to improve the signal-to-noise ratio.

The data in the XANES region of the absorption coefficient were examined by applying the same procedure for pre-edge line fitting, postedge curve fitting, and edge-step normalization to all data. XANES and EXAFS data processing and analysis were performed using the IFEFFIT package. EXAFS data modeling and analysis was performed using standard procedures.[46,47] The passive electron reduction factor was obtained to be 0.90 ± 0.06 from the fit to the Rh foil data and fixed to be 0.90 in the analysis of all Rh catalysts. Several parameters describing electronic properties, specifically, the correction to the photoelectron energy origin, and local structural environment (coordination number (N), bond length (R), and mean squared disorder parameter (σ^2) of the nearest neighbors) around absorbing atoms were varied in the fit.

Several models were compared for quantitative analysis of the EXAFS data. The best fit to the temperature dependent data was obtained assuming the combination of Rh−O and Rh−Co contributions. Theoretical EXAFS signals were constructed using FEFF6 theory for these contributions, and their structural parameters (N, R, and σ^2) were varied in the fits of theory to the data.

Catalytic Measurements. Twenty-one milligrams of 60−80 mesh catalysts were mixed with the same size SiO_2 (0.5−10 μm, 99%, Aldrich) to make up the catalyst bed volume of 1 cm^3. They were loaded into a plug-in fixed-bed flow microreactor. Nitric oxide, hydrogen, and argon were premixed and then flowed into a quartz tube. Blank experiments showed no activity in NO reduction with H_2 in the temperature range of 25 °C−300 °C. Products were mainly analyzed with a gas chromatograph. Conversion of NO was calculated with the equation

$$X\% = \frac{N_{NO} - N^T_{NO}}{N_{NO}}$$

The N^T_{NO} is the number of moles of NO detected at a reaction temperature. N_{NO} stands for the number of moles of NO introduced before catalysis. Selectivity to production of N_2 was calculated with the equation

$$S\% = \frac{2N^T_{N_2}}{N_{NO} - N^T_{NO}}$$

The $N^T_{N_2}$ is the number of moles of N_2 detected at a reaction temperature.

3. RESULTS AND DISCUSSION

3.1. Characterization of As-Synthesized Rh_1/Co_3O_4 Catalyst before Catalysis. Co_3O_4 nanorods with singly dispersed Rh atoms were synthesized with three steps. The preparation starts from synthesis of Co_3O_4 nanorods as described in Experimental Section. The second and third steps are the impregnation of Rh^{3+} ions onto the surface of

dx.doi.org/10.1021/cs300816u | ACS Catal. 2013, 3, 1011−1019

Co_3O_4 nanorods and a followed on-site reduction of electrostatically adsorbed Rh^{3+} using $NaBH_4$, respectively. Figure 1

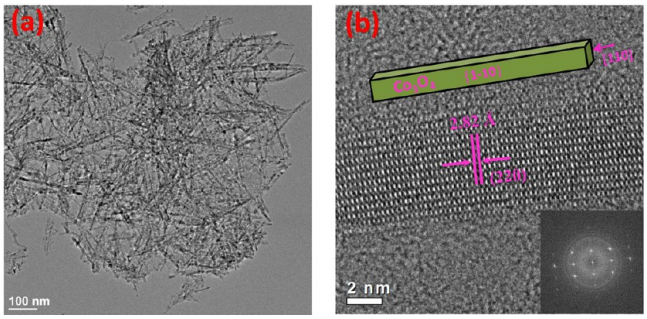

Figure 1. TEM images of pure Co_3O_4 nanorods: (a) large scale image; (b) high-resolution image.

presents TEM images of Co_3O_4 nanorods with diameters of 5−8 nm and different lengths (50−200 nm). XRD performed with a synchrotron beam wavelength (λ= 0.3196 Å) (Supporting Information, Figure S1) showed the crystallization of Co_3O_4 nanorods.

Aqueous solution of $Rh(NO_3)_3$ was added to Co_3O_4 nanorods dispersed in methanol. Under the assumption that all Rh atoms are dispersed on the surface of Co_3O_4 nanords, the ratio of Rh atoms to the Co atoms of the topmost surface layer of Co_3O_4 is ∼1.2% or so. Stirring makes Rh^{3+} dispersed onto the surface of Co_3O_4 nanorods. The third step is the reduction of the weakly bound Rh^{3+} by adding $NaBH_4$. $NaBH_4$ is a strong reducing agent. Rh^{3+} impregnated on the surface of Co_3O_4 nanorods is reduced. As Rh^{3+} ions are originally weakly bound to OH groups or oxygen atoms on Co_3O_4 nanorods, Rh^0 atoms formed through on-site reduction will immediately bind to oxygen atoms of its neighboring OH groups or oxygen atoms of the Co_3O_4 surface, forming Rh−O bonds locally. The low concentration of Rh^{3+} makes Rh atoms anchor on Co_3O_4 surface separately.

The formation of Co_3O_4 with singly dispersed Rh atoms was evidenced by the EXAFS studies to be discussed in the following paragraph. ICP measurements show that the atomic ratio of Rh to Co is 0.14%, basically consistent with the molar ratio of precursors: $Rh(NO_3)_3$ to $Co(CH_3COO)_2$ used in synthesis, 0.1%. Here Rh_1/Co_3O_4 refers to Co_3O_4 anchored with singly dispersed Rh atoms.

Figure 2 presents the TEM images of the Rh_1/Co_3O_4 catalyst. The as-synthesized Rh_1/Co_3O_4 catalyst basically retains the morphology of pure Co_3O_4 nanorods, a diameter of ∼5 nm with a length of 50 nm−200 nm (Figure 1). The high

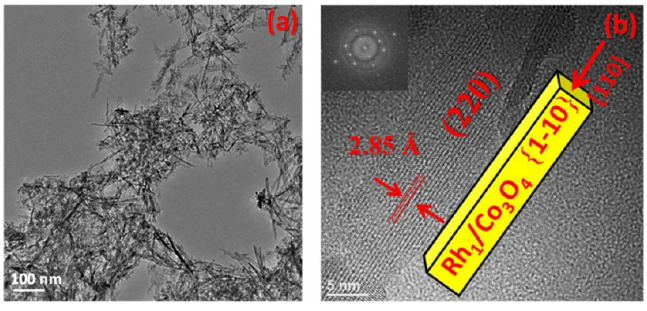

Figure 2. TEM images of Rh_1/Co_3O_4: (a) large scale; (b) high-resolution image.

resolution image (Figure 2b) of Rh_1/Co_3O_4 clearly shows the crystallization of the Co_3O_4 phase. The measured interplanar distance, 2.82 Å, is exactly the value of (220) reported in the literature.[40] We tried to use aberration-corrected annular dark-field scanning transmission electron microscopy (ADF-STEM) to distinguish Rh from Co_3O_4 nanorods. However, the difference in atomic numbers between Rh and Co is not large enough to make the HAADF-STEM imaging technique distinguish Rh atoms from Co atoms of Co_3O_4.

Alternatively, EXAFS can identify the dispersion of Rh atoms through measurement of the coordination number of cobalt atoms and oxygen atoms surrounding Rh in Rh_1/Co_3O_4 as-synthesized and during catalysis. The exposed surface of Co_3O_4 (110) has Co^{3+} and O^{2-} if we assume the preferentially exposed surface is a B-type surface which has Co^{3+} and O^{2-}.[48] Rh^{3+} could anchor on O^{2-} or OH of the surface. Visual examination of the EXAFS data (Figure 3a) was used as a basis for the followed model for quantitative analysis. No sign of Rh−Rh contributions was found. Indeed, the presence of Rh−Rh contribution would be revealed as the first peak position in bulk Rh data but such contribution is missing in the data. Rh−O contributions are missing in the high temperature data (≥220 °C). Indeed, the data collected at room temperature and the 90 °C data have a peak at much shorter distance than those at higher temperatures. The data at 25 °C−90 °C and high temperature are consistent with Rh−O and Rh−Co, respectively.

In quantitative analysis, we verified these preliminary conclusions by fitting either individual Rh−O, Rh−Co, and Rh−Rh contributions, or their combinations, to all data sets. Representative fits of the EXAFS data are shown in Figure 4. The fits demonstrated that the data collected at room temperature and 300 °C data are dominated by Rh−O (Figure 4a) and Rh−Co contributions (Figure 4b), respectively. The coordination numbers, bond lengths, and their disorders for the Rh−O and Rh−Co bonds of the as-synthesized catalysts are listed in Table 1. We confirmed that the best fits corresponded to the model where no Rh atoms directly bonded to either Rh atom or Co atoms in the as-synthesized Rh_1/Co_3O_4 at room temperature. This suggests that each Rh atom bonds to oxygen atoms of the Co_3O_4 surface instead of a Co or Rh atom. We also ruled out a possibility that Rh adopts a local structure of a rhodium oxide. In Figure 4c, the second peak in Rh_2O_3 oxide (the reference sample for comparison) appears at around 2.7 Å. This peak corresponds to the Rh−Rh coordination shell of the 3.0 Å in radius, in agreement with the crystal structure of Rh_2O_3. For Rh_1/Co_3O_4 (black line in Figure 4c), there is no significant contribution at that position, and the entire region is smeared, indicating multiple contributions that are much less coherent than in the oxide structure. This is more consistent with single dispersed Rh atoms than Rhodium oxides.

The oxidation states of Rh atoms on the Co_3O_4 surface were investigated with Rh K-edge XANES. Figure 5a shows the Rh K-edge XANES data of Rh_1/Co_3O_4 and Rh foil. A comparison of rhodium in Rh_2O_3 or as-synthesized Rh_1/Co_3O_4 is present in Figure 5b. The cationic state of rhodium in the as-synthesized catalyst is clearly evident from the raw data (Figures 5a) and is very similar to the oxidation state (+3) in Rh_2O_3 (Figure 5b). From the quantitative analysis of EXAFS data and comparison with reference Rh_2O_3 data, we ruled out formation of Rh_2O_3 nanoclustes though rhodium in Rh_1/Co_3O_4 has an oxidation state of +3. This conclusion is consistent with the XPS studies (Figure 6). As shown in Figure 6a, the binding energy, 308.6

dx.doi.org/10.1021/cs300816u | ACS Catal. 2013, 3, 1011−1019

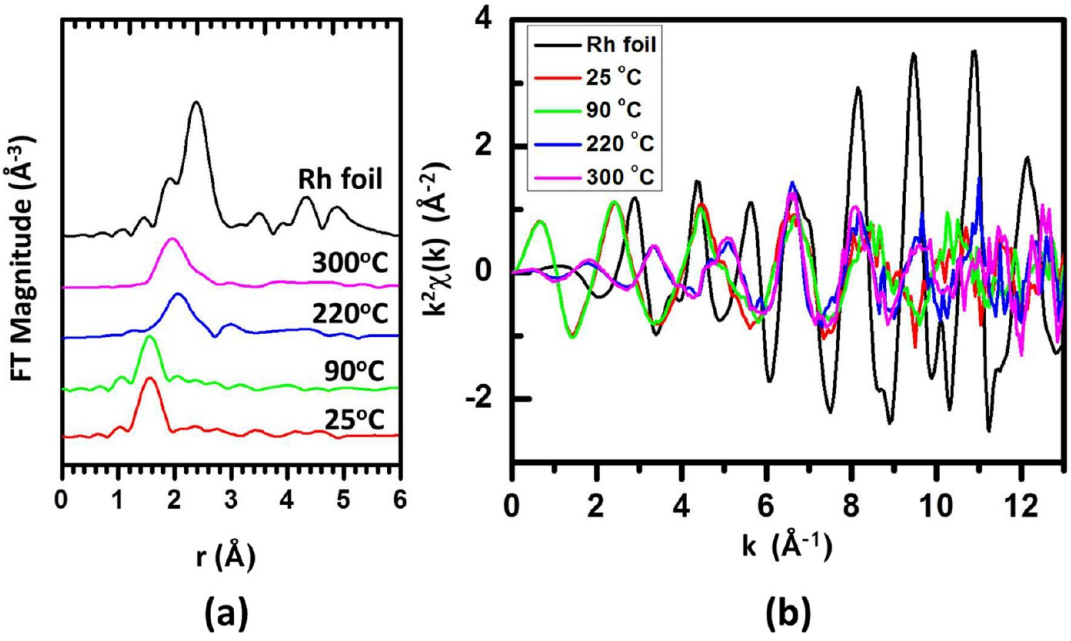

Figure 3. In situ EXAFS studies of Rh_1/Co_3O_4 under different conditions: r-space (a) and k-space (b) data of the k^2-weighted Rh K-edge EXAFS spectra. The k-range from 2 $Å^{-1}$ to 11 $Å^{-1}$ was used in all Fourier transforms. In situ studies were performed at different reaction temperatures.

eV, of Rh $3d_{5/2}$ of the as-synthesized single-atom dispersed catalyst at 25 °C clearly shows the nature of oxidizing valence state of rhodium atoms instead of metallic Rh. Obviously, the binding of Rh to oxygen atoms makes it upshift by 1.5 eV in contrast to metallic Rh.[49] The Co 2p photoemission feature (Figure 6b) is similar to that of pure Co_3O_4 (Supporting Information, Figure S3). A weak shoulder at 789.9 eV is attributed to the satellite peak of Co $2p_{3/2}$ of Co^{3+} in octahedral sites.[50] The absence of a satellite peak at 786.7 eV of Co $2p_{3/2}$ of Co^{2+} on octahedral sites of CoO further suggests the nature of Co_3O_4.[51] The O 1s photoemission feature (Figure 6c) is contributed from the lattice oxygen atom and nonstoichiometric oxygen vacancies.[51] Overall, those studies suggested that Rh^{3+} exists on Co_3O_4 through bonding with oxygen and they are singly dispersed on Co_3O_4.

3.2. Catalytic Performance for Reduction of Nitric Oxide with Hydrogen. Catalytic performance of Rh_1/Co_3O_4 was performed in a fixed-bed microflow reactor. Twenty-one milligrams of Rh_1/Co_3O_4 catalyst was dispersed on quartz powder. A mixture gas of NO and H_2 and Ar was introduced into the reactor. Partial pressure ratio of NO and H_2 is 1:1. Products were analyzed with a GC. Figure 7a presents the catalytic performance of Rh_1/Co_3O_4 at different temperatures *without* a pretreatment in reactant gases. At 140 °C, this catalyst exhibits conversion of NO at 4%. It increases to 26% at 180 °C. It rapidly increases to 93% at 220 °C and reaches 100% at 260 °C. In terms of selectivity of production of N_2, it is 3% and 56% at 200 and 220 °C, respectively. It reaches 88% at 260 °C. A highest selectivity of 97% is reached at 300 °C. Notably, Rh_1/Co_3O_4 without any pretreatments (Figure 7a2) has much higher selectivity to production of N_2 in the temperature of 200 °C−300 °C in contrast to pure Co_3O_4 without any pretreatments at the same temperature (Figure 7a2). Thus, the singly dispersed Rh atoms play a crucial role in the much higher selectivity in production of N_2 in contrast to that on pure Co_3O_4 nanorods.

Catalytic studies of Rh_1/Co_3O_4 that experienced a pretreatment at 300 °C in the mixture of reactant gases and a followed cooling to 150 °C were performed. Figure 7b lists the measured catalytic performance in the temperature regime of 150 °C-300 °C upon the pretreatment (annealing to 300 °C in the mixture of reactant gases and then cooling to 150 °C in the same gaseous environment). Conversion (Figure 7b1) and selectivity (Figure 7b2) at 150 °C are 3% and 0%, respectively. Selectivities to N_2 at 180 and 200 °C are 76% and 88%, respectively (Figure 7b2), which are significantly different than 0% and 3% at these temperatures on Rh_1/Co_3O_4 without a pretreatment at 300 °C in the reactant mixture (Figure 7a2). This distinct difference shows the pretreatment (annealing to 300 °C in the mixture of reactants) produces different active sites. This active site(s) exhibits a high selectivity at low temperatures (180 °C−260 °C) (Figure 7b2). The catalyst (Rh_1/Co_3O_4) upon this pretreatment at 300 °C exhibits a better catalytic performance in reduction of nitric oxide with H_2 than Rh supported on other oxides.[19]

3.3. In Situ Studies of Rh_1/Co_3O_4 Catalyst. Chemical environment of Rh atoms in Rh_1/Co_3O_4 catalysts during catalysis was studied with AP-XPS, EXAFS, and XANES. EXAFS studies were performed at 25 °C, 90 °C, 220 °C, and 300 °C in a flow microreactor in which a mixture of reactants (1 bar, NO:H_2 = 1:1) flows through catalyst bed (0.1 g 60−80 mesh catalyst). Thus, the chemistry of catalysts identified with in situ EXAFS can exactly present the chemistry of the catalyst during the catalytic measurements in a flow microreactor in our catalysis lab. Figure 3 presents r-space and k-space data of the k^2-weighted Rh K-edge EXAFS spectra of Rh_1/Co_3O_4 at room temperature in ambient condition and during catalysis. Figure 4c shows EXAFS of both Rh_2O_3 and the as-synthesized Rh_1/Co_3O_4 at 25 °C. However, the raw EXAFS data (Figures 3a and 3b) showed a shift of the first nearest neighbor peak to larger distances at 220 °C in contrast to that at 25 °C. Analysis of EXAFS data attributed this effect to the significant changes in coordination environment of Rh atoms that is experienced at 220 °C in the mixture of reactants. It suggests a restructuring of singly dispersed Rh atoms and its neighboring atoms at this temperature regime. Table 1 shows Rh atoms retain their single

dx.doi.org/10.1021/cs300816u | *ACS Catal.* 2013, 3, 1011−1019

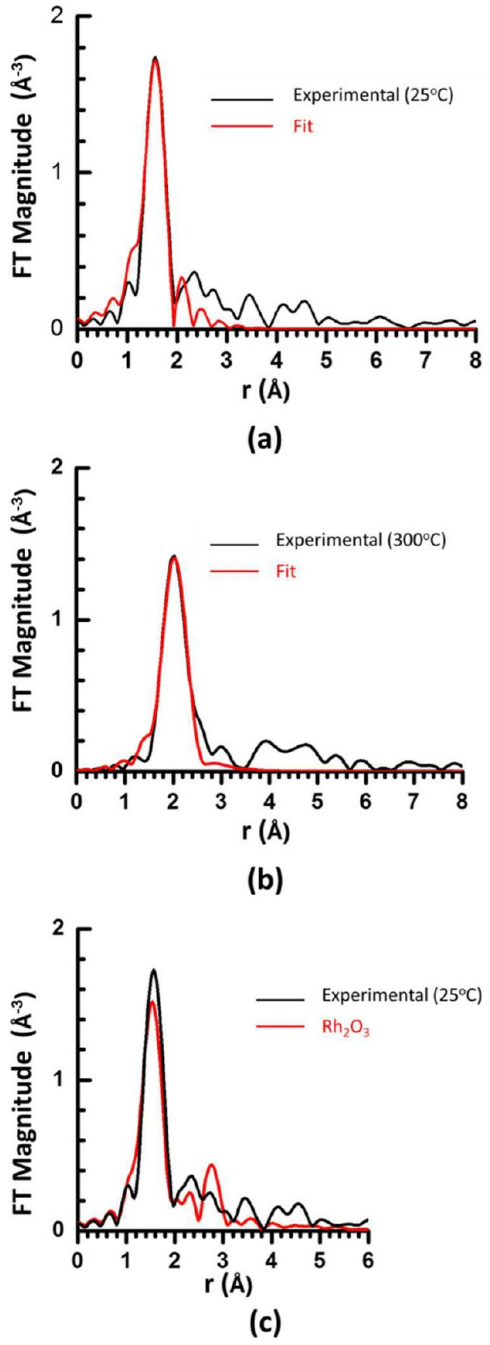

Figure 4. In situ EXAFS data and theoretical fits of Rh_1/Co_3O_4 catalyst at 25 °C (a) and 300 °C (b), and comparison between the raw data of Rh_2O_3 and the as-synthesized Rh_1/Co_3O_4 catalyst at room temperature (c). In situ studies were performed at a pressure of 1 bar. The molar ratio of NO and H_2 is 1:1. The balance gas is 1:1.

distribution and bond with Co atoms instead of oxygen atoms at 220 and 300 °C. This is consistent with the rapid increase of catalytic selectivity at 220 °C (Figure 7a2). The correlation between restructuring of Rh_1/Co_3O_4 during catalysis at 220 °C (Table 1) and the simultaneous rapid increase of catalytic selectivity (Figure 7b2) suggest that the new chemical environment of Rh atoms is favorable for the selective reduction of NO to N_2. Based on the coordination environment of Rh measured with in situ EXAFS, this cluster is a singly dispersed nanocluster, $RhCo_n$.

Under these same conditions of catalytic measurements in the temperature regime of 25 °C−300 °C, there is no Rh−Rh bond formed in the whole temperature range based on in situ EXAFS studies (Figure 3 and Table 1). It suggests that these Rh atoms on the surface of Co_3O_4 retain their single dispersion up to 300 °C during the catalysis. At 90 °C, both Rh−O and Rh−Co bonds were identified. The coordination number of Co to Rh is 4.6 ± 2.1. It seems that Rh−Co bonds are formed through a loss of surface oxygen atoms upon reaction with H_2. The loss of surface lattice oxygen atoms of Co_3O_4 at a temperature higher than 90 °C makes Rh bond with four neighboring cobalt atoms though it originally bonded with surface lattice oxygen atoms. An easy removal of oxygen atoms on Co_3O_4 was suggested as the driving force of the high activity of CO oxidation at a low temperature and low energy barrier in hopping of oxygen vacancies of Co_3O_4 based on DFT calculation.[48] The difference in chemical environment of Rh atoms of our catalyst between 25 and 90 °C (Table 1) suggests that surface restructuring has already started at 90 °C.

A direct evidence for the loss of oxygen atoms bonded to Rh atoms is the coordination number of oxygen atoms around a Rh atom, N(Rh−O) at 220 °C (Table 1), which is in fact zero. Obviously, the original binding of a Rh atom to oxygen atoms experienced a large change with the increase of reaction temperatures to 220 °C. Upon a surface, lattice oxygen atom is abstracted by an external species such as H_2 or H; the Rh atom tends to bond with four cobalt atoms to form a cluster as shown in Figure 8a. This cluster, $RhCo_n$ is in the surface layer. Removal of oxygen atoms around Rh atoms does not result in the aggregation of Rh atoms which have chemically bonded to oxygen before pretreatment in H_2+NO or H_2. Upon removal of some oxygen atoms bonded to a Rh atom, Rh atoms can immediately bond to the Co atoms underneath which lose one or more oxygen atoms. The immediate bonding with Co atoms is thermodynamically and kinetically favorable in contrast to moving to another Rh atom which is 2−3 nm far on average. In fact, the coverage of Rh on Co atoms on the surface a Co_3O_4 nanorod is about 1.2% for a catalyst with starting ratio of Rh to Co of 0.1% if we assume all Rh atoms are dispersed on surfaces of Co_3O_4 nanorods. Such a large separation prevents an aggregation. The formation of singly dispersed $RhCo_n$ nanoclusters on Co_3O_4 during catalysis at 200 °C−300 °C is

Table 1. Coordination Numbers, Bond Lengths, and Their Disorders of Rh and Its Nearest Neighboring Atoms of Rh_1/Co_3O_4 at 25 °C, 90 °C, 220 °C, and 300 °C in the Mixture of NO and H_2 Studied with EXAFS

T(°C)	N(Rh−O)	N(Rh -Co)	R(Rh−O), Å	R(Rh−Co), Å	σ^2(Rh−O), Å^2	σ^2(Rh−Co), Å^2
25	3.8 ± 0.8		2.05 ± 0.03		<0.0021[a]	
90	3.9 ± 0.6	4.6 ± 2.1	2.05 ± 0.01	2.53 ± 0.01	<0.0050[a]	0.022 ± 0.006
220		3.2 ± 0.8		2.52 ± 0.02		0.004 ± 0.002
300		4.8 ± 1.1		2.50 ± 0.02		0.007 ± 0.002

[a]Only the upper limit could be obtained for these values from the fit.

dx.doi.org/10.1021/cs300816u | ACS Catal. 2013, 3, 1011−1019

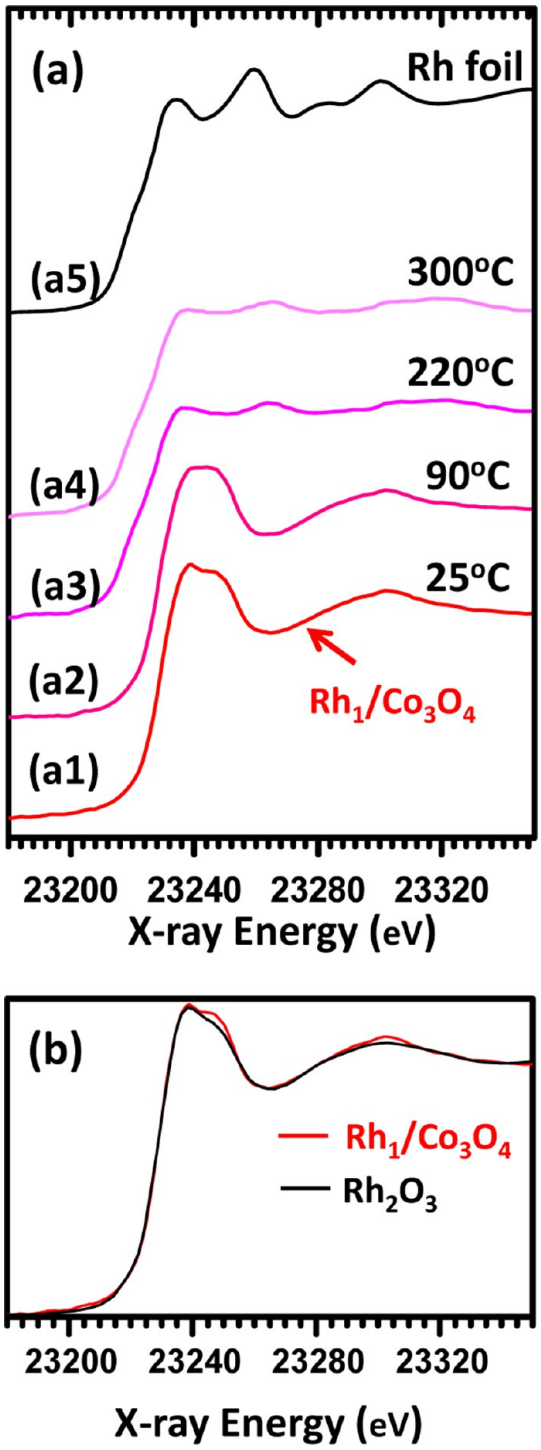

Figure 5. Rh K-edge XANES of catalysts during catalysis. (a) Rh K-edge XANES data of Rh_1/Co_3O_4 during catalysis in the mixture of reactant gases in the temperature regime of 25 °C−300 °C. (b) Rh K-edge XANES data of Rh_2O_3 (black line) and the as-synthesized Rh_1/Co_3O_4 (red line).

evidenced by EXAFS data. $RhCo_n$ nanoclusters could aggregate and form large clusters if the coverage of $RhCo_n$ nanoclusters is high or the temperature of the catalyst is higher than 300 °C. EXAFS studies show $RhCo_n$ remains a singlet at a temperature of 300 °C or a lower temperature. Thus, the low surface concentration of Rh in the topmost surface layer of Co_3O_4 and the mild catalysis conditions makes $RhCo_n$ nanoclusters singly dispersed on Co_3O_4 at a temperature up to 300 °C.

The evolution of Co 2p and Rh 3d of Rh_1/Co_3O_4 under different reaction conditions was studied by using the in-house AP-XPS in our group. There is no significant change of the photoemission feature of Co 2p at different reaction temperatures up to 300 °C in the mixture of NO and H_2 with a ratio of 1:1 (Figure 9a). It suggests there was no significant restructuring of the subsurface of Co_3O_4 although $RhCo_n$ nanoclusters were formed on the topmost surface at 220 °C during catalysis (also called pretreatment here). Notably, a down-shift of Rh 3d photoemission peaks along the increase of the reaction temperatures from 25 to 220 °C (marked with green lines) was observed in Figure 9b, probably because of the formation of a new configuration, $RhCo_n$ nanoclusters of Rh atom at ∼220 °C under reaction conditions. In this case, Rh is still at an oxidizing state. The high binding energy (308.6 eV) of Rh atom in $RhCo_n$ embedded in the topmost layer of Co_3O_4 nanorods results from a few factors. One is electron transfer from rhodium atom to oxygen atom through a cobalt atom (Rh→Co→O) since each Co atom of a $RhCo_n$ nanocluster is bonded with a few oxygen atoms.

As shown in Supporting Information, Figure S4 and reported in reference 51, the photoemission feature of Co 2p of Co^{2+} in the octahedral sites of rock-salt CoO exhibits characteristic satellite peaks of Co^{2+} in octahedral coordination with oxygen atoms at 786.4 and 803.1 eV corresponding to Co $2p_{3/2}$ and Co $2p_{1/2}$, respectively. Whether Co_3O_4 is partially reduced to CoO under reaction conditions of a mixture of NO and H_2 can be identified by checking whether there are such satellite peaks of Co^{2+} in octahedral coordination with oxygen atoms. The lack of a pair of satellite peaks at 786.4 and 803.1 eV in Co 2p photoemission features in the temperature regime of catalytic measurements (25 °C−300 °C) (Figure 9a) clearly shows the preservation of the Co_3O_4 phase up to 300 °C. In fact, the photoemission feature of Co 2p of Rh_1/Co_3O_4 at 300 °C in the mixture of NO and H_2 is in good agreement with that of Co_3O_4 reported.[51]

Figure 10 presents the atomic ratio of O/Co of Rh_1/Co_3O_4 under reaction conditions. The ratio was calculated under an assumption that oxygen vacancies of Co_3O_4 are filled with OH group from dissociation of H_2O and thus O/Co ratio of Rh_1/Co_3O_4 at room temperature is 1.33. The error bar in the measurements of O 1s and Co 2p peak areas is 5%. Notably, the O/Co ratio at 220 °C is lower than that at 25 °C by ∼0.20. The low O/Co ratio at 220 and 300 °C clearly suggested the loss of some oxygen atoms when a Rh_1/Co_3O_4 catalyst was annealed to 220 and 300 °C in the mixture of NO and H_2. The loss of oxygen atoms partially results from the removal of oxygen atoms bonded to Rh ions of the surface layer, supported by in situ EXAFS studies.

These in situ studies clearly show a restructuring of surface of Rh_1/Co_3O_4 from singly distributed Rh atoms mainly bonded with oxygen atoms in an as-synthesized catalyst to singly distributed $RhCo_n$ nanoclusters at 220 and 300 °C supported on Co_3O_4. Oxygen vacancies were identified on the surface of Co_3O_4 though Co_3O_4 is not transformed to CoO. The preservation of Co_3O_4 could result from the mixture reducing reactant H_2 and oxidizing NO.

3.4. Catalysis on Singly Dispersed $RhCo_n$ Nanoclusters. It seems a potential oxidation of NO to NO_2 by surface oxygen atoms of Co_3O_4 at low temperature could decrease the selectivity for production of N_2; from this point of

dx.doi.org/10.1021/cs300816u | ACS Catal. 2013, 3, 1011−1019

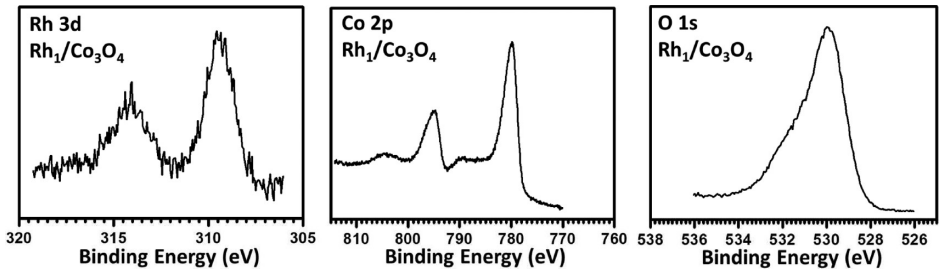

Figure 6. Photoemission feature of Rh 3d, Co 2p, and O 1s of the as-synthesized Rh_1/Co_3O_4 at room temperature in vacuum.

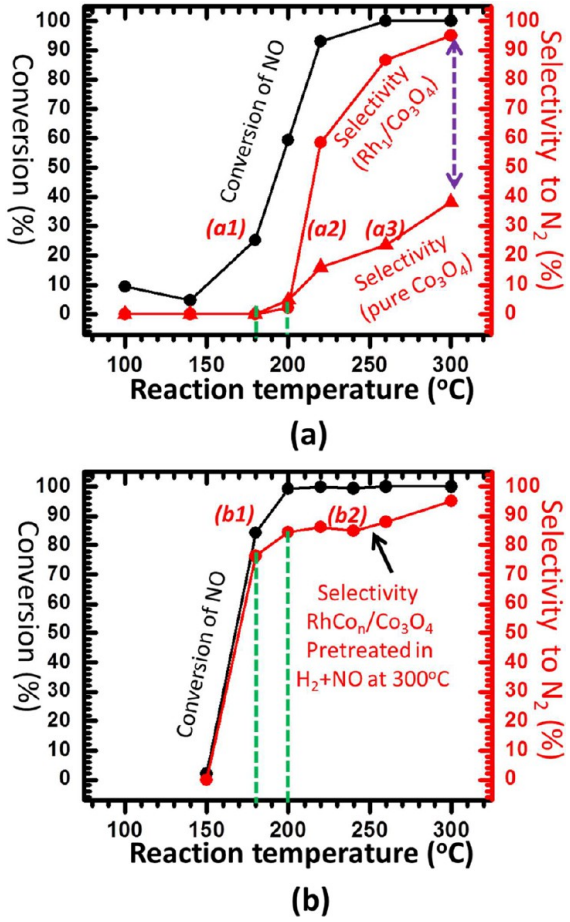

Figure 7. Catalytic performances of Rh_1/Co_3O_4 and pure Co_3O_4. **a1**: conversion of Rh_1/Co_3O_4 without pretreatment; **a2**: selectivity of Rh_1/Co_3O_4 without pretreatment; **a3**: selectivity of pure Co_3O_4 without pretreatment. **b1**: conversion of Rh_1/Co_3O_4 upon pretreatment at 300 °C in a mixture of reaction gases (NO:H_2 = 1:1); **b2**: selectivity of Rh_1/Co_3O_4 upon pretreatment at 300 °C in a mixture of reaction gases (NO:H_2 = 1:1).

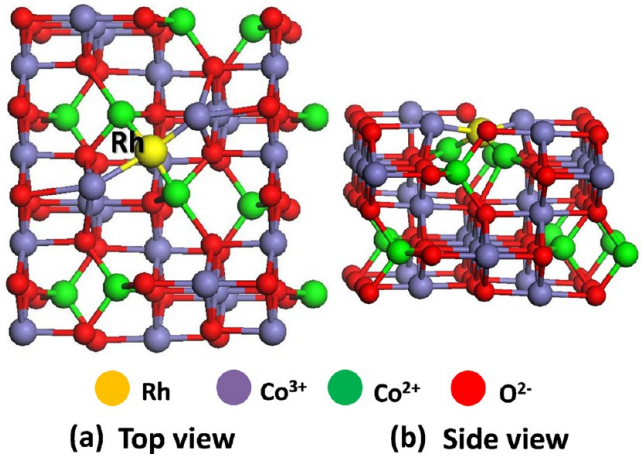

Figure 8. Structural model of a singly dispersed $RhCo_n$ nanocluster formed through restructuring in a mixture of reactant gases at 220 °C.

view the formation of surface oxygen vacancies at high temperature could block the channel of production of NO_2 through oxidation of NO by a surface lattice oxygen atom and thus enhance selectivity to production of N_2. Since the density of oxygen vacancies is increased upon annealing to high temperature in reactant gas the higher selectivity to N_2 on Rh_1/Co_3O_4 with an annealing to 300 °C in contrast to that without any annealing (Figure 7a2) potentially results from the loss of surface oxygen during annealing. To elucidate whether the formed oxygen vacancies at a high temperature contributes to the promotion of selectivity to N_2, additional experiments were performed. Pure Rh_1/Co_3O_4 was pretreated in H_2 of 1 Torr at 220 °C for 2 h. AP-XPS confirmed the atomic ratio of oxygen to cobalt is ∼1.10 upon pretreatment and it is still a Co_3O_4 phase. Thus, pretreatment in H_2 at 220 °C essentially generated almost the same density of oxygen vacancies for Co_3O_4 as that of Rh_1/Co_3O_4 pretreated in a mixture of H_2 and NO at 300 °C. The followed catalytic measurement on Co_3O_4 with H_2 pretreatment at 220 °C exhibits selectivities (Supporting Information, Figure S5b) very similar to those without H_2 pretreatment (Figure 7a3 or Supporting Information, Figure S5a); this similarity in selectivity suggests that the lack of oxygen atoms (or the increase of oxygen vacancies) is not a factor of the enhancement of selectivity to N_2 upon a pretreatment in reactant mixture at 300 °C. Furthermore, it shows enhancement of selectivity to N_2 on $RhCo_n/Co_3O_4$ upon annealing at 300 °C in the reactant mixture (Figure 7b2) is not due to the low concentration of surface oxygen atoms. Thus, we would deduce the promotion of selectivity for Rh_1/Co_3O_4 upon pretreatment in reactants results from the formation of new site, $RhCo_n$ nanoclusters.

Regarding Co_3O_4, oxygen atoms of the Co_3O_4 (110) surface can be released in CO oxidation even at a temperature as low as −70 °C.[40] Co^{3+} ions on the surface of pure Co_3O_4 nanorods could be sites for dissociation of NO[52] and H_2 molecules . A dissociated nitrogen atom from this nitric oxide can spill over and then bond with another nitrogen atom to form a nitrogen molecule. Hydrogen atoms dissociated on Co^{3+} can couple with surface lattice oxygen atom(s) from dissociation of NO, forming a H_2O molecule; the generated oxygen vacancies can absorb oxygen atoms from dissociation of NO molecules in next catalytic cycle.

In terms of catalysis on restructured Rh_1/Co_3O_4 (termed $RhCo_n/Co_3O_4$), a $RhCo_n$ nanocluster acts as a site to dissociate

dx.doi.org/10.1021/cs300816u | ACS Catal. 2013, 3, 1011−1019

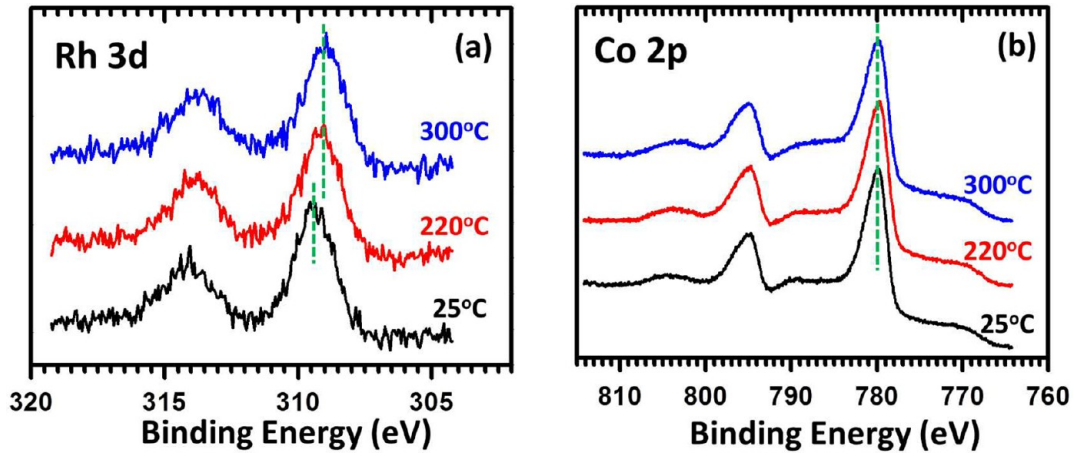

Figure 9. In situ AP-XPS studies of Co 2p (a) and Rh 3d (b) of the as-synthesized Rh_1/Co_3O_4 at different reaction temperatures in the mixture 50% NO and 50% H_2.

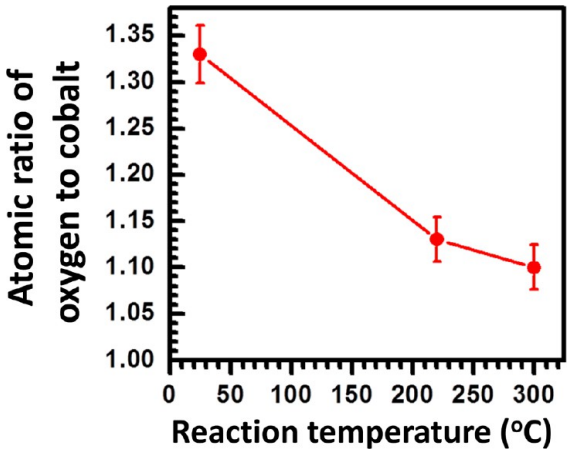

Figure 10. Atomic ratio of oxygen atoms to cobalt atoms in the surface region of Rh_1/Co_3O_4 in the mixture of NO and H_2 at different reaction temperatures measured with AP-XPS.

a NO molecule. The role of Rh atom is somewhat similar to the reduction of NO with H_2 on a Rh nanoparticle;[6,53−55] Supporting Information Figures S6, S7, and S8 schematically show three possible reaction pathways of NO + H_2 on the $RhCo_n/Co_3O_4$ catalyst. It is noted that they are potential mechanisms proposed on the basis of the above experimental observations. Further investigation through collaboration with a computational group is being planned. In Supporting Information, Figure S6, Co^{3+} is a site for H_2 dissociation. On the other hand, Rh atom of a $RhCo_n$ nanocluster could actually act as a site to dissociate a NO molecule. The oxygen atom from NO dissociation will spill over and couple with hydrogen atoms dissociated by Co^{3+}, forming a H_2O molecule. A nitrogen atom from NO dissociation can spill over and couple with another nitrogen atom to form a N_2 molecule. Alternatively, as shown in Supporting Information, Figure S7, hydrogen atoms dissociated from H_2 on a cobalt atom can spill over to oxygen atom near to the Co atom, forming a H_2O molecule. Thus, an oxygen vacancy is generated (Supporting Information, Figure S7e). It is filled with an oxygen atom dissociated from a NO molecule. In this case, surface lattice oxygen atoms participate into the reaction.

Another potential pathway is schematically shown in Supporting Information, Figure S8. Rh atom acts as a site of H_2 dissociation. A nitric oxide molecule is absorbed by an oxygen vacancy. Thus, the N−O bond is weakened. The dissociated nitrogen atom will spill over and couple with another nitrogen atom, forming a N_2 molecule (Supporting Information, Figure S8e). A surface lattice oxygen atom will couple with two hydrogen atoms dissociated from H_2 on Rh to form a H_2O molecule. Both the potential pathways in Supporting Information, Figures S7 and S8 involve oxygen vacancies.

4. SUMMARY

Co_3O_4 with singly dispersed Rh atoms was synthesized with an on-site reduction upon the impregnation of Rh^{3+} on the Co_3O_4 surface. EXAFS showed the single dispersion of Rh atoms on Co_3O_4 in as-synthesized Rh_1/Co_3O_4 since the coordination number of Rh−Rh, N(Rh−Rh) is zero in the as-synthesized catalyst, Rh_1/Co_3O_4. In situ characterizations of Rh_1/Co_3O_4 showed that Rh atoms exist in $RhCo_n$ singly dispersed in the surface layer of Co_3O_4 nanorods during catalysis up to 300 °C. The active sites are singly dispersed $RhCo_n$ nanoclusters generated through restructuring of Rh_1/Co_3O_4 at about 220 °C in the mixture of reactant gases. This new catalytic phase exhibits a high selectivity for the production of N_2 in the reduction of NO with H_2 in the temperature range of 180 °C−300 °C. This study shows that in situ studies allow for building a direct correlation between catalytic performances and the corresponding surface chemistry and structure during catalysis. This correlation significantly aids understanding of catalytic performance and identification of new catalytic sites formed during catalysis.

■ ASSOCIATED CONTENT

Supporting Information

Synthesis of Co_3O_4 nanorods. Co 2p photoemission features of pure Co_3O_4 nanorods and pure CoO formed through reduction of pure Co_3O_4 in H_2. Catalytic selectivity to production of N_2 on pure Co_3O_4 without and with pretreatment in H_2. Potential reaction pathways of reduction of NO with H_2 on $RhCo_n/Co_3O_4$. This material is available free of charge via the Internet at http://pubs.acs.org.

AUTHOR INFORMATION

Corresponding Author

*E-mail: ftao@nd.edu.

Present Address

[⊥]Institute of Process Engineering, Chinese Academy of Sciences, Beijing 100190, China.

Author Contributions

[∥]These authors contributed to this work equally.

Notes

The authors declare no competing financial interest.

ACKNOWLEDGMENTS

This work is supported by the Chemical Sciences, Geosciences and Biosciences Division, Office of Basic Energy Sciences, Office of Science, U.S. Department of Energy, under the Grant DE-FG02-12ER1635. XANES and EXAFS studies were supported by the Chemical Sciences, Geosciences and Biosciences Division, Office of Basic Energy Sciences, Office of Science, U.S. Department of Energy under the Grant DE-FG02-03ER15476 (from A.F.). L.W. acknowledges financial support from The Li Foundation. Beamline X18B at the NSLS is supported in part by the Synchrotron Catalysis Consortium, U.S. Department of Energy Grant DE-FG02-05ER15688. We thank R. Palomino of Brookhaven National Laboratory for sharing the raw X-ray absorption data in Rh_2O_3.

REFERENCES

(1) Li, Y., Somorjai., G. A. *Introduction to Surface Chemistry and Catalysis*, 2nd ed.; Wiley: Hoboken, NJ, 2010.
(2) Granger, P.; Parvulescu, V. I. *Chem. Rev.* **2011**, *111*, 3155.
(3) Tomita, A.; Yoshii, T.; Teranishi, S.; Nagao, M.; Hibino, T. *J. Catal.* **2007**, *247*, 137.
(4) Park, S. M.; Jang, H.-G.; Kim, E. S.; Han, H.-S.; Seo, G. *Appl. Catal., A* **2012**, *427*, 155.
(5) Hasegawa, Y.; Haneda, M.; Kintaichi, Y.; Hamada, H. *Appl. Catal., B* **2005**, *60*, 41.
(6) Newton, M. A.; Dent, A. J.; Diaz-Moreno, S.; Fiddy, S. G.; Evans, J. *Angew. Chem., Int. Ed.* **2002**, *41*, 2587.
(7) Okumura, K.; Motohiro, T.; Sakamoto, Y.; Shinjoh, H. *Surf. Sci.* **2009**, *603*, 2544.
(8) Engelmann-Pirez, M.; Granger, P.; Leclercq, G. *Catal. Today* **2005**, *107−08*, 315.
(9) Ren, Y.; Harold, M. P. *ACS Catal.* **2011**, *1*, 969.
(10) Paredis, K.; Ono, L. K.; Behafarid, F.; Zhang, Z.; Yang, J. C.; Frenkel, A. I.; Cuenya, B. R. *J. Am. Chem. Soc.* **2011**, *133*, 13455.
(11) Qi, G. S.; Yang, R. T.; Rinaldi, F. C. *J. Catal.* **2006**, *237*, 381.
(12) Dhainaut, F.; Pietrzyk, S.; Granger, P. *Catal. Today* **2007**, *119*, 94.
(13) Biniwale, R. B.; Pande, J. V.; Dhakad, M.; Labhsetwar, N. K.; Ichikawa, M. *Catal. Lett.* **2008**, *123*, 164.
(14) Costa, C. N.; Efstathiou, A. M. *Appl. Catal., B* **2007**, *72*, 240.
(15) Dhainaut, F.; Pietrzyk, S.; Granger, P. *Appl. Catal., B* **2007**, *70*, 100.
(16) Burch, R.; Coleman, M. D. *Appl. Catal., B* **1999**, *23*, 115.
(17) Qiao, B.; Wang, A.; Yang, X.; Allard, L. F.; Jiang, Z.; Cui, Y.; Liu, J.; Li, J.; Zhang, T. *Nat. Chem.* **2011**, *3*, 634.
(18) Hamada, H.; Haneda, M. *Appl. Catal., A* **2012**, *421*, 1.
(19) Savva, P. G.; Costa, C. N. *Catal. Rev.-Sci. Eng.* **2011**, *53*, 91.
(20) Granger, P.; Dhainaut, F.; Pietrzik, S.; Malfoy, P.; Mamede, A. S.; Leclercq, L.; Leclercq, G. *Top. Catal.* **2006**, *39*, 65.
(21) Furfori, S.; Russo, N.; Fino, D.; Saracco, G.; Specchia, V. *Chem. Eng. Sci.* **2010**, *65*, 120.
(22) Costa, C. N.; Savva, P. G.; Andronikou, C.; Lambrou, P. S.; Polychronopoulou, K.; Belessi, V. C.; Stathopoulos, V. N.; Pomonis, P. J.; Efstathiou, A. M. *J. Catal.* **2002**, *209*, 456.
(23) Costa, C. N.; Stathopoulos, V. N.; Belessi, V. C.; Efstathiou, A. M. *J. Catal.* **2001**, *197*, 350.
(24) Machida, M.; Ikeda, S.; Kurogi, D.; Kijima, T. *Appl. Catal., B* **2001**, *35*, 107.
(25) Polshettiwar, V.; Varma, R. S. *Green Chem.* **2010**, *12*, 743.
(26) Gunter, P. L. J.; Niemantsverdriet, J. W.; Ribeiro, F. H.; Somorjai, G. A. *Catal. Rev.-Sci. Eng.* **1997**, *39*, 77.
(27) Iablokov, V.; Beaumont, S. K.; Alayoglu, S.; Pushkarev, V. V.; Specht, C.; Gao, J.; Alivisatos, A. P.; Kruse, N.; Somorjai, G. A. *Nano Lett.* **2012**, *12*, 3091.
(28) Huang, W.; Liu, J. H.-C.; Alayoglu, P.; Li, Y.; Witham, C. A.; Tsung, C.-K.; Toste, F. D.; Somorjai, G. A. *J. Am. Chem. Soc.* **2010**, *132*, 16771.
(29) Somorjai, G. A.; Park, J. Y. *Top. Catal.* **2008**, *49*, 126.
(30) Feng, L.; Hoang, D. T.; Tsung, C.-K.; Huang, W.; Lo, S. H.-Y.; Wood, J. B.; Wang, H.; Tang, J.; Yang, P. *Nano Res.* **2011**, *4*, 61.
(31) Tsung, C.-K.; Kuhn, J. N.; Huang, W.; Aliaga, C.; Hung, L.-I.; Somorjai, G. A.; Yang, P. *J. Am. Chem. Soc.* **2009**, *131*, 5816.
(32) Joo, S. H.; Park, J. Y.; Tsung, C.-K.; Yamada, Y.; Yang, P.; Somorjai, G. A. *Nat. Mater.* **2009**, *8*, 126.
(33) Rioux, R. M.; Komor, R.; Song, H.; Hoefelmeyer, J. D.; Grass, M.; Niesz, K.; Yang, P.; Somorjai, G. A. *J. Catal.* **2008**, *254*, 1.
(34) Sun, Y. G.; Xia, Y. N. *Nano Lett.* **2003**, *3*, 1569.
(35) Mostafa, S.; Behafarid, F.; Croy, J. R.; Ono, L. K.; Li, L.; Yang, J. C.; Frenkel, A. I.; Cuenya, B. R. *J. Am. Chem. Soc.* **2010**, *132*, 15714.
(36) Narayanan, R.; El-Sayed, M. A. *Nano Lett.* **2004**, *4*, 1343.
(37) Narayanan, R.; El-Sayed, M. A. *J. Phys. Chem. B* **2005**, *109*, 12663.
(38) Jin, M.; Zhang, H.; Xie, Z.; Xia, Y. *Energy Environ. Sci.* **2012**, *5*, 6352.
(39) Zhang, H.; Jin, M.; Liu, H.; Wang, J.; Kim, M. J.; Yang, D.; Xie, Z.; Liu, J.; Xia, Y. *ACS Nano* **2011**, *5*, 8212.
(40) Xie, X.; Li, Y.; Liu, Z.-Q.; Haruta, M.; Shen, W. *Nature* **2009**, *458*, 746.
(41) Tao, F. *Chem. Commun.* **2012**, *48*, 3812.
(42) Tao, F.; Salmeron, M. *Science* **2011**, *331*, 171.
(43) Zhu, Y.; Zhang, S.; Ye, Y.; Zhang, X.; Wang, L.; Zhu, W.; Cheng, F.; Tao, F. *ACS Catal.* **2012**, *2*, 2403.
(44) Wen, C.; Zhu, Y.; Ye, Y.; Zhang, S.; Cheng, F.; Liu, Y.; Wang, P.; Tao, F. *ACS Nano* **2012**, *6*, 9305.
(45) Nashner, M. S.; Frenkel, A. I.; Adler, D. L.; Shapley, J. R.; Nuzzo, R. G. *J. Am. Chem. Soc.* **1997**, *119*, 7760.
(46) Frenkel, A. I.; Hills, C. W.; Nuzzo, R. G. *J. Phys. Chem. B* **2001**, *105*, 12689.
(47) Sanchez, S. I.; Menard, L. D.; Bram, A.; Kang, J. H.; Small, M. W.; Nuzzo, R. G.; Frenkel, A. I. *J. Am. Chem. Soc.* **2009**, *131*, 7040.
(48) Jiang, D.-e.; Dai, S. *Phys. Chem. Chem. Phys.* **2011**, *13*, 978.
(49) Moulder, J. F. S., W., F.; Sobol, P. E.; Bomben, K. D. *Handbook of X-ray Photoelectron Spectroscopy*; Perkin-Elmer Corporation: Eden Prairie, MN, 1992.
(50) Petitto, S. C.; Marsh, E. M.; Carson, G. A.; Langell, M. A. *J. Mol. Catal A: Chem.* **2008**, *281*, 49.
(51) Chuang, T. J.; Brundle, C. R.; Rice, D. W. *Surf. Sci.* **1976**, *59*, 413.
(52) Xu, X.-L.; Yang, E.; Li, J.-Q.; Li, Y.; Chen, W.-K. *ChemCatChem* **2009**, *1*, 384.
(53) Papp, H.; Sabde, D. P. *Appl. Catal., B* **2005**, *60*, 65.
(54) Tomishige, K.; Asakura, K.; Iwasawa, Y. *J. Catal.* **1995**, *157*, 472.
(55) Hong, L.; Hesse, M.; Imbihl, R. *J. Phys. Chem. C* **2009**, *113*, 4174.